Original Article

MOLECULAR METABOLISM

FGF15/19 is required for adipose tissue plasticity in response to thermogenic adaptations

Samantha Morón-Ros [1,2], Iker Uriarte [3,4], Carmen Berasain [3,4], Matías A. Avila [3,4], Mònica Sabater-Masdeu [2,5], José María Moreno-Navarrete [2,5], José Manuel Fernández-Real [2,5], Marta Giralt [1,2], Francesc Villarroya [1,2,], Aleix Gavaldà-Navarro [1,2,*]**

ABSTRACT

Objective: To determine the role of enterokine FGF15/19 in adipose tissue thermogenic adaptations.
Methods: Circulating FGF19 and gene expression (qRT-PCR) levels were assessed in subcutaneous adipose tissue from obese human patients. Effects of experimentally increased FGF15 and FGF19 levels in vivo were determined in mice using adenoviral and adeno-associated vectors. Adipose tissues were characterized in FGF15-null mice under distinct cold-related thermogenic challenges. The analyses spanned metabolic profiling, tissue characterization, histology, gene expression, and immunoblot assays.
Results: In humans, FGF19 levels are directly associated with UCP1 gene expression in subcutaneous adipose tissue. Experimental increases in FGF15 or FGF19 induced white fat browning in mice as demonstrated by the appearance of multilocular beige cells and markers indicative of a beige phenotype, including increased UCP1 protein levels. Mice lacking FGF15 showed markedly impaired white adipose tissue browning and a mild reduction in parameters indicative of BAT activity in response to cold-induced environmental thermogenic challenges. This was concomitant with signs of altered systemic metabolism, such as reduced glucose tolerance and impaired cold-induced insulin sensitization.
Conclusions: Enterokine FGF15/19 is a key factor required for adipose tissue plasticity in response to thermogenic adaptations.

Keywords Adipose tissue plasticity; Browning; Enterokine; Fibroblast Growth Factor 15; Fibroblast Growth Factor 19

1. INTRODUCTION

FGF15 (and its human orthologue, FGF19) are members of the FGF protein family; they are produced by ileal enterocytes and belong to the subfamily of endocrine FGFs, together with FGF21 and FGF23. FGF15/19 synthesis in ileal enterocytes is stimulated by bile acids that, through FXR, induce transcription of the FGF15/19 genes. FGF15/19 acts on target cells through FGF receptors, mostly FGFR4, that are predominantly expressed in the liver [1]. Similar to FGF21, the action of FGF15/19 requires the interaction of FGFRs with the co-receptor β-Klotho (KLB). The main recognized function of FGF15/19 is to regulate bile acid homeostasis through its ability to inhibit the expression of CYP7A1, which is the key enzyme in the hepatic biosynthesis of bile acids from cholesterol [2]. FGF15/19 also participates in regulating hepatic metabolism, and in the liver, FGF19 reportedly triggers effects that resemble the action of insulin, such as enhanced glycogenesis and protein synthesis [3]. FGF19 has also been shown to promote hepatocarcinogenesis [4] and favor fatty liver regeneration [5].

Brown adipose tissue (BAT) activation and the acquisition of brown fat-like properties by white adipose tissue (WAT; that is, the so-called "browning" of WAT) are associated with enhanced energy expenditure and protection against obesity and damaging metabolic conditions such as hyperglycemia and hyperlipidemia [6]. High thermogenic requirements, such as those experienced under cold environment exposure or diet-originating stimuli, induce BAT activity and WAT browning. Although the sympathetic nervous system is considered to be the main driver of thermogenic BAT activation and WAT browning, growing evidence indicates that non-sympathetic regulators are also involved [7]. Among them, FGF21 has been identified as being involved in eliciting BAT activity and WAT browning, although its relative contribution to the cold- or diet-induced thermogenic activation of adipose tissue remains a matter of debate and ongoing research [8].

[1]Department of Biochemistry and Molecular Biomedicine and Institute of Biomedicine, University of Barcelona, Institut de Recerca Sant Joan de Déu, Esplugues de Llobregat, Barcelona, Spain [2]CIBEROBN, Carlos III Health Institute, Spain [3]Hepatology Program, CIMA, University of Navarra, IdiSNA, Pamplona, Spain [4]CIBEREHD, Carlos III Health Institute, Spain [5]Department of Diabetes, Endocrinology and Nutrition, de Girona Biomedical Research Institute (IdIBGi), Girona, Spain

*Corresponding author. Aleix Gavaldà-Navarro, Molecular Metabolism and Disease, Department of Biochemistry and Molecular Biomedicine, School of Biology, Institute of Biomedicine (IBUB), University of Barcelona, Avda Diagonal 643 (Edifici Prevosti, Planta-1), 08028, Barcelona, Spain. Tel.: +34934021549. E-mail: aleixgavalda@ub.edu (A. Gavaldà-Navarro).

**Corresponding author. Francesc Villarroya, Molecular Metabolism and Disease, Department of Biochemistry and Molecular Biomedicine, School of Biology, Institute of Biomedicine (IBUB), University of Barcelona, Avda Diagonal 643 (Edifici Prevosti, Planta-1), 08028, Barcelona, Spain. Tel.: +34934021525. E-mail: fvillarroya@ub.edu (F. Villarroya).

Received August 20, 2020 • Revision received November 2, 2020 • Accepted November 4, 2020 • Available online 7 November 2020

https://doi.org/10.1016/j.molmet.2020.101113

Several observations support the idea that there is cross-talk between the intestine and thermogenic activation of adipose tissues. Manipulation of the intestinal microbiota has been reported to influence BAT activity and WAT browning in distinct experimental settings [9,10,11,12]. The endocrine factor GLP-1 originating in the intestine is known to induce BAT thermogenic activity and browning, mostly through an indirect hypothalamus-mediated mechanism [13]. The gut hormone secretin was recently shown to target BAT and elicit satiation signaling [14]. Bariatric surgery is known to rapidly improve patients' glucose/insulin homeostasis [15] and cause BAT activation [16], possibly due to gut-originating signals that are not yet fully understood. The induction of FG15/19 has been proposed to contribute to such an effect [17]. By using a large cohort of patients representing a wide range of BMI, we identified a significant reciprocal correlation between BMI and circulating FGF19 levels as well as a direct correlation between plasma FGF19 levels and the expression of UCP1, which is a marker gene for WAT browning.

Using the FGF15-null mouse model and gain-of-function approaches based on FGF15 overexpression, we show that FGF15/19 plays a key role in adaptive WAT browning.

2. MATERIALS AND METHODS

2.1. Human studies

Plasma and abdominal subcutaneous WAT samples were prospectively collected from obese patients who underwent different surgical procedures (cholecystectomy, abdominal hernia, and gastric bypass) as well as non-obese healthy volunteers. Patients with hepatic diseases (tumors or hepatitis C infection) or thyroid disorders were excluded. All the subjects were recruited by the Endocrinology Service at Dr. Josep Trueta Hospital (Girona, Spain). All of the participants were of Caucasian origin, were assessed in the post-absorptive state, and reported that their body weight had been stable for at least three months before the study. This study was conducted in accordance with the Declaration of Helsinki. Dr. Josep Trueta Hospital's ethical committee approved the protocol, and all the patients provided written informed consent before their inclusion after the purpose of the study was explained to them. Samples and data from patients included in this study were provided by the FATBANK platform promoted by the CIBEROBN and coordinated by the IDIBGI Biobank (Biobanc IDIBGI, B.0000872) integrated in the Spanish National Biobanks Network and processed following standard operating procedures with the appropriate approval of the Ethics, External Scientific, and FATBANK Internal Scientific committees. Anthropometrical characteristics and circulating biochemical parameters are described in Supplementary Table 1. Adipose samples were obtained under sterile conditions, rinsed with PBS, frozen in liquid nitrogen, and stored at −80 °C. Body mass index (BMI) was calculated according to the formula: weight/height^2 (kg/m^2). Body fat mass was measured by bioelectrical impedance. An extensive panel of metabolic and hormonal parameters in plasma (Supplemental Table 1) was analyzed at the certified core biochemistry laboratory at Dr. Josep Trueta Hospital. FGF19 protein levels in plasma were quantified by ELISA (RD191107200R; Biovendor, Brno, Czech Republic).

2.2. Mouse studies

2.2.1. Mouse care

Mice were bred in the animal research facilities at the University of Barcelona. The animals were provided a standard chow diet (Teklad 2018 global 18% protein; Envigo, Indianapolis, IN, USA) and water ad libitum and maintained in a temperature-controlled environment on a 12/12 h light—dark cycle. Energy intake was calculated by weighing their food every week and assuming an energy density of 13 kJ/g. All experiments involving animals were conducted in accordance with European Community Council Directive 86/609/EEC and the National Institutes of Health guidelines for the care and use of laboratory animals. All experimental procedures were approved by the Institutional Animal Care and Use Committee of the University of Barcelona.

2.2.2. Overexpression of FGF15 and FGF19 in vivo

Three-month-old C57BL/6J mice received a single retro-orbital injection with 2×10^{11} VP/mouse of Ad5-control or Ad5-FGF15 ($n = 5$) as previously described [18] or a single retro-orbital injection with 1×10^{10} VP/mouse of AAV8-control or AAV8-FGF19 ($n = 6$) as previously described [4]. The mice were analyzed 1 week or 3 weeks post-injection, respectively.

2.2.3. Studies involving Fgf15-null mice

The Fgf15-null mice and WT littermate controls were on a mixed C57BL/6Jx129/Sv strain background as previously described [18]. Three-month-old WT and Fgf15-null mice ($n = 6$) were housed under standard conditions (21 °C) or transferred to a cold chamber or a temperature-controlled animal contention unit (UAN-I, TDI, Madrid, Spain) and maintained at 4 °C or 30 °C, respectively, for 1 week.

2.2.4. Thermography

Surface temperatures were recorded using a T335 infrared digital thermal imaging camera (FLIR Systems, Wilsonville, OR, USA). The mice were shaved at the measurement sites 48 h before thermographic measurements. The resulting images were analyzed using FLIR Quick Report 1.2 software (FLIR Systems). The maximal temperature from the interscapular area corresponding to iBAT sites was retrieved. The core temperature was determined with rectal temperature measurement using a KM-1420 temperature recorder (Kane-May Measuring Instruments, Hertfordshire, UK).

2.2.5. Mouse sampling

The mice were killed by decapitation. Their blood was collected in heparinized tubes for plasma preparation. The liver, subcutaneous (inguinal depot), and visceral (epididymal depot) WAT and interscapular BAT were removed, weighed, immediately frozen in liquid nitrogen, and stored at −80 °C until processing.

For histological analysis, adipose tissues were fixed with 4% paraformaldehyde for 24 h and stored in 70% ethanol until paraffin blocking preparation. Paraffin-embedded tissue sections (3 μm thick) were generated, air dried, further dried overnight at 60 °C, and subjected to hematoxylin and eosin staining. Lipid droplet areas, brown adipocyte count, and iWAT adipocyte areas were measured using open-source ImageJ software with the Adiposoft plugin as described in [19].

For immunohistofluorescence staining, paraffin-embedded tissue sections were deparaffinated and rehydrated and heat-induced antigen retrieval was performed in sodium citrate buffer. Slides were washed in TBS 1× with 0.025% Triton X-100, blocked in 10% normal serum with 1% BSA in TBS for 2 h at room temperature (RT), and incubated with primary rabbit anti-UCP1 antibody 1/500 (ab10983; Abcam plc, Cambridge, UK) in TBS with 1% BSA overnight at 4 °C. After rinsing the slides in TBS 0.025% Triton X-100, the slides were incubated with goat anti-rabbit Alexa 488 secondary antibody (A27034; Thermo Fisher Scientific Inc., Rockford, IL, USA) 1/2000 in TBS with 1% BSA for 1 h at RT, rinsed with TBS, stained with 50 μg/ml of propidium iodide

solution (P4864; Sigma–Aldrich, Saint Louis, MO) for 15 min, and mounted. Fluorescent images were obtained using a Leica DFC 360FX camera coupled to a Leica DMIRE2 microscope.

2.2.6. Mouse measurements of circulating parameters

Blood glucose was quantified using the Accutrend System (Roche Diagnostics GmbH, Mannheim, Germany). Circulating metabolites and hormones were determined from mouse plasma using commercially available kits against the following: triglycerides (TR0100; Sigma–Aldrich), non-esterified fatty acids (434-91795 and 436-91995; Wako Chemicals GmbH, Neuss, Germany), total bile acids (80470; Crystal Chem Inc., Elk Grove Village, IL, USA), insulin (10-1247-01; Mercodia AB, Uppsala, Sweden), FGF21 (RD291108200R; Biovendor), and CXCL14/BRAK (SEB607Mu; Cloud-Clone Corp., Katy, TX, USA). For glucose tolerance tests, glucose in aqueous solution was administered intraperitoneally (2.5 g glucose/kg) to overnight-fasted mice, blood was obtained from the tail 0, 15, 30, 45, 60, 90, 120, and 150 min after glucose injection, and glycemia was measured.

2.3. Western blotting

Frozen BAT and subcutaneous WAT were homogenized in RIPA buffer (50 mM of Tris HCl pH 7.4, 150 mM of NaCl, 1 mM of EDTA, 1% v/v Triton X-100, and 0.1% SDS) containing a protease inhibitor cocktail (Roche) and phosphatase inhibitors (2 mM of sodium orthovanadate, 1 mM of sodium pyrophosphate, and 10 mM of sodium fluoride). Lysates were centrifuged at 16,000 g at 4 °C for 10 min. The protein concentration was measured using a bicinchoninic acid (BCA) protein assay as specified by the manufacturer (Pierce, Thermo Fisher Scientific, Inc.), and the samples were stored at −80 °C until they were used. The samples were resolved by SDS-polyacrylamide gel electrophoresis and transferred to nitrocellulose membranes. The membranes were blocked for 1 h at RT in TBST (10 mM of Tris pH 7.4, 140 mM of sodium chloride, and 0.1% Tween20) containing 3% BSA. Primary antibodies were applied overnight at 4 °C in TBST-3% BSA. After incubation with HRP-labeled secondary antibodies for 1 h at RT in TBST-3% BSA, the membranes were developed with an ECL system and their luminescence was detected using a Fujifilm LAS-3000 CCD imaging system (GE Healthcare, Chicago, IL, USA). For quantification, images were acquired and quantified using Multi Gauge V3.0 (Fujifilm). The primary antibodies utilized and their dilutions were as follows: rabbit anti-UCP1 1/1000 (ab10983; Abcam), rabbit anti-tyrosine hydroxylase 1/1000 (AB152; EMD Millipore, Temecula, CA, USA), and mouse anti-β-actin 1/1000 (A1978; Sigma–Aldrich).

2.4. RNA isolation, cDNA synthesis, and real-time PCR

Dissected tissues from mice (liver, BAT, and WAT) or human subcutaneous adipose tissue were homogenized using a Tissue Lyser LT (Qiagen, Germany). Total RNA from homogenized tissues was isolated using a column affinity-based method (NucleoSpin RNA II; Macherey–Nagel, Düren, Germany). Total RNA (500 ng) was transcribed into cDNA using TaqMan reverse-transcription reagents (Applied Biosystems/Life Technologies, Foster City, CA, USA). For quantitative analysis of mRNA expression, a TaqMan quantitative real-time polymerase chain reaction (qPCR) was performed on a 7500 Real-Time PCR System (Applied Biosystems) using the specific primer pair/probe sets presented in Supplemental Table 12. Relative mRNA levels of target genes were normalized with respect to that of mouse *Ppia* (Mm02342430_g1) or human *PPIA* (Hs04194521_s1) using the comparative ($2^{-\Delta CT}$) method. Transcript levels were considered undetectable in cases when the CT value was >40 under our experimental conditions.

2.5. Statistical analysis

Statistical analyses were conducted using GraphPad Prism software version 5.03 (GraphPad Software Inc., San Diego, CA, USA). Student's t-test, Mann–Whitney test, and two-way ANOVA with Tukey or Dunnett post hoc corrections were applied. Correlation was established based on linear regression analysis. Differences at $P \leq 0.05$ were considered significant. *$P \leq 0.05$, **$P \leq 0.01$, and ***$P \leq 0.001$.

3. RESULTS

3.1. Plasma FGF19 levels positively correlate with the expression of the brown/beige marker gene UCP1 in human subcutaneous adipose tissue

FGF19 levels were assessed in a cohort of individuals (n = 98) spanning a wide range of BMI from morbid obesity to normal weight (for anthropometrical data, see Supplemental Table 1). Our data indicated that there was a significant inverse correlation of FGF19 levels with BMI and fat mass (Figure 1A) in agreement with previous reports [20]. These correlations were age- and gender-independent (Supplemental Table 2). Biopsies of subcutaneous adipose tissue were obtained in a subset of individuals (n = 50). The expression levels of marker genes for distinct processes associated with adipose tissue physiopathology were analyzed and their correlations with FGF19 levels were determined. Interestingly, the transcript levels of *UCP1*, which is a marker gene for the brown/beige adipose tissue phenotype, showed a statistically significant positive correlation with circulating FGF19 levels (Figure 1B). Another marker gene of the BAT/beige phenotype, such as *DIO2*, also showed a (non-significant) trend toward positive correlation, whereas the transcript levels of genes encoding general adipogenesis-related actors, such as adiponectin, *PPARG*, *FASN*, or *PLIN1* (Figure 1B) did not correlate with circulating FGF19 levels. The association between circulating FGF19 and *UCP1* mRNA levels in SAT lost statistical significance when adjusted for BMI, suggesting that this association was closely related to the status of individuals in relation to obesity condition.

3.2. Overexpression of FGF15 and FGF19 causes browning of WAT

The previously described findings prompted us to directly determine the potential effects of FGF15/19 on adipose tissues in relation to browning and thermogenesis-related adaptations in a mouse model. Considering the marked differences between murine FGF15 and human FGF19 orthologues [21], we used a totally species-homologous experimental approach to directly determine whether FGF15 can promote browning of adipose tissues in mice. In the absence of a commercially available recombinant FGF15 protein, we injected a single retro-orbital dose of an adenoviral vector to deliver a full-length FGF15-encoding construct (Ad-FGF15) whose hepatic expression and delivery is a commonly used tool to increase specific protein levels in plasma [22]. At 1 week post-injection, transcript analysis revealed that the mRNA level of *Fgf15* was induced more than 100-fold in the liver over the almost undetectable basal level (Supplemental Table 3). Moreover, the expression of the hepatic FGF15 target gene *Cyp7a1* was strongly repressed, demonstrating that the injection increased the biological action of FGF15. Injection with Ad-FGF15 did not significantly modify body weight, adipose depot size, biochemical parameters such as glycemia, insulinemia, or triglyceridemia, or the hepatic expression of *Fgf21* (Supplemental Table 3).

The experimental increase in FGF15 did not trigger any alterations in BAT in terms of histological morphology (that is, the lipid droplet size and number of adipocytes) (Figure 2A), the profile of thermogenesis-related gene expression (Figure 2B and Supplemental Table 3),

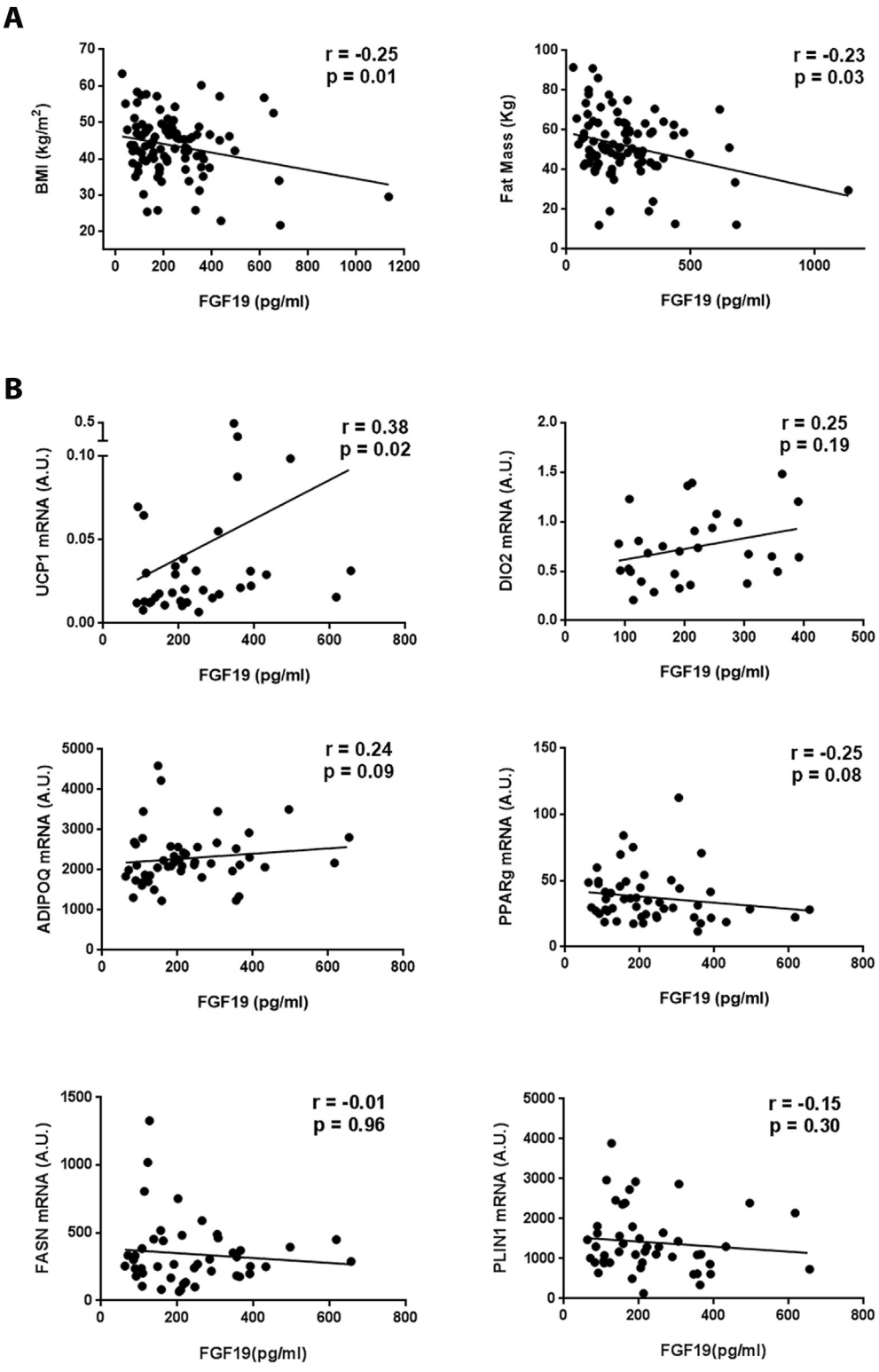

Figure 1: Circulating FGF19 protein levels positively correlate with the expression of the browning marker gene UCP1 in subcutaneous adipose tissue of humans. Correlation between FGF19 protein levels in plasma from obese patients, (A) BMI and fat mass (n = 98), and (B) mRNA levels of *UCP1*, *DIO2*, *ADIPOQ*, *PPARG*, *FASN*, and *PLIN1* in subcutaneous adipose tissue (n = 50). All correlations were analyzed using Spearman's correlation except for BMI, which was analyzed by Pearson's correlation (n = 38).

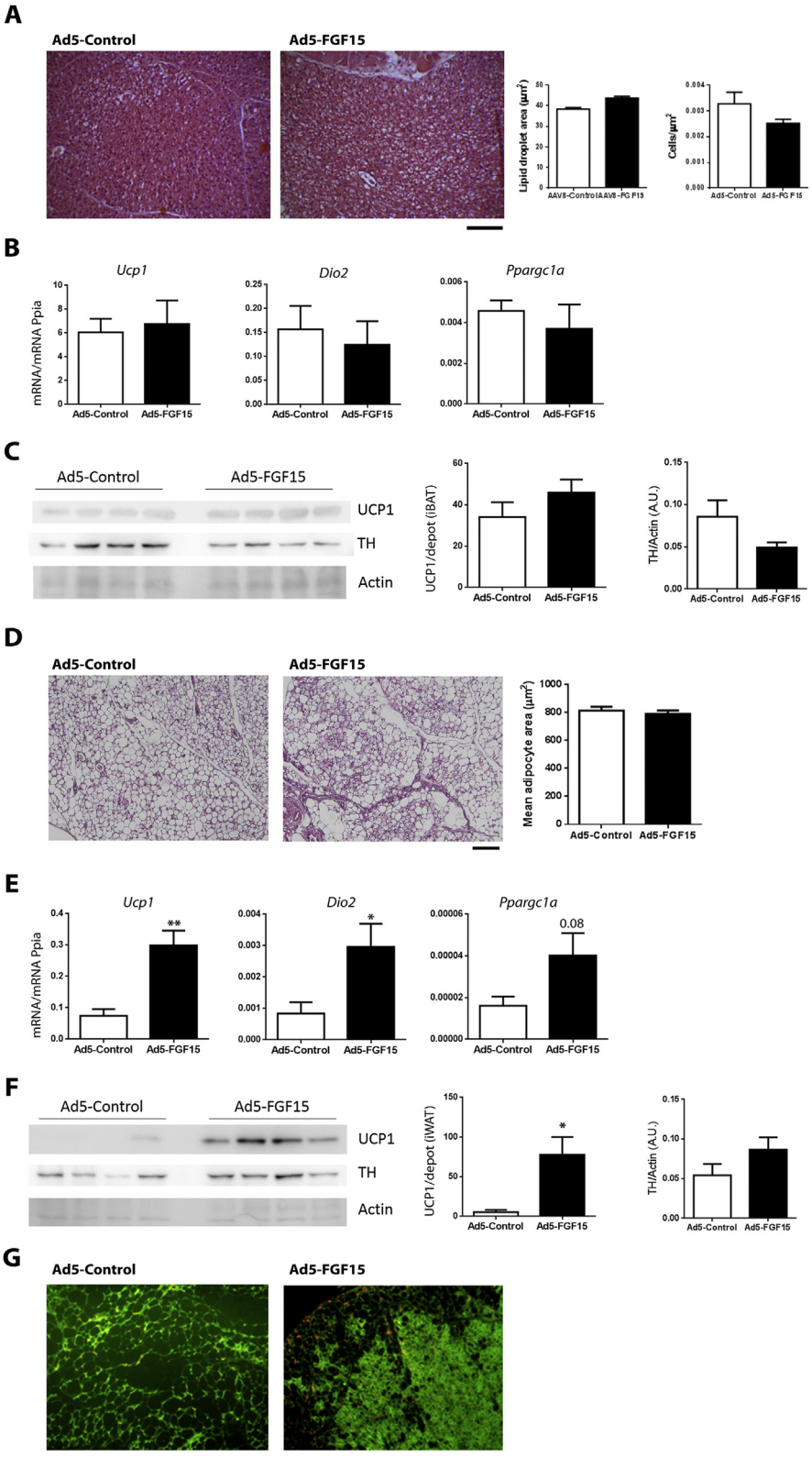

Figure 2: Overexpression of FGF15 promotes browning of subcutaneous white adipose tissue in mice. All data were obtained from 3-month-old C57BL/6J mice subjected to adenovirus-mediated overexpression of FGF15 for 1 week. Representative hematoxylin and eosin-stained histological sections of (A) brown (BAT) (20×) and quantification of lipid droplet areas and BAT density, (D) subcutaneous white (iWAT) adipose tissues (10×), and quantification of adipocyte areas. Scale: 100 µm mRNA levels of *Ucp1*, *Dio2*, and *Ppargc1a* in (B) BAT and (E) iWAT. Representative image of UCP1 protein immunodetection and protein levels of UCP1 per depot in (C) BAT and (F) iWAT. Actin immunodetection was used as a loading control. (G) UCP1 (green) and nucleus (red) immunohistofluorescence staining in iWAT. Bars indicate mean ± SEM (n = 6). *P ≤ 0.05 and **P ≤ 0.01 denote statistical significance for comparisons between Ad-control and Ad-FGF15 analyzed by Student's t-test.

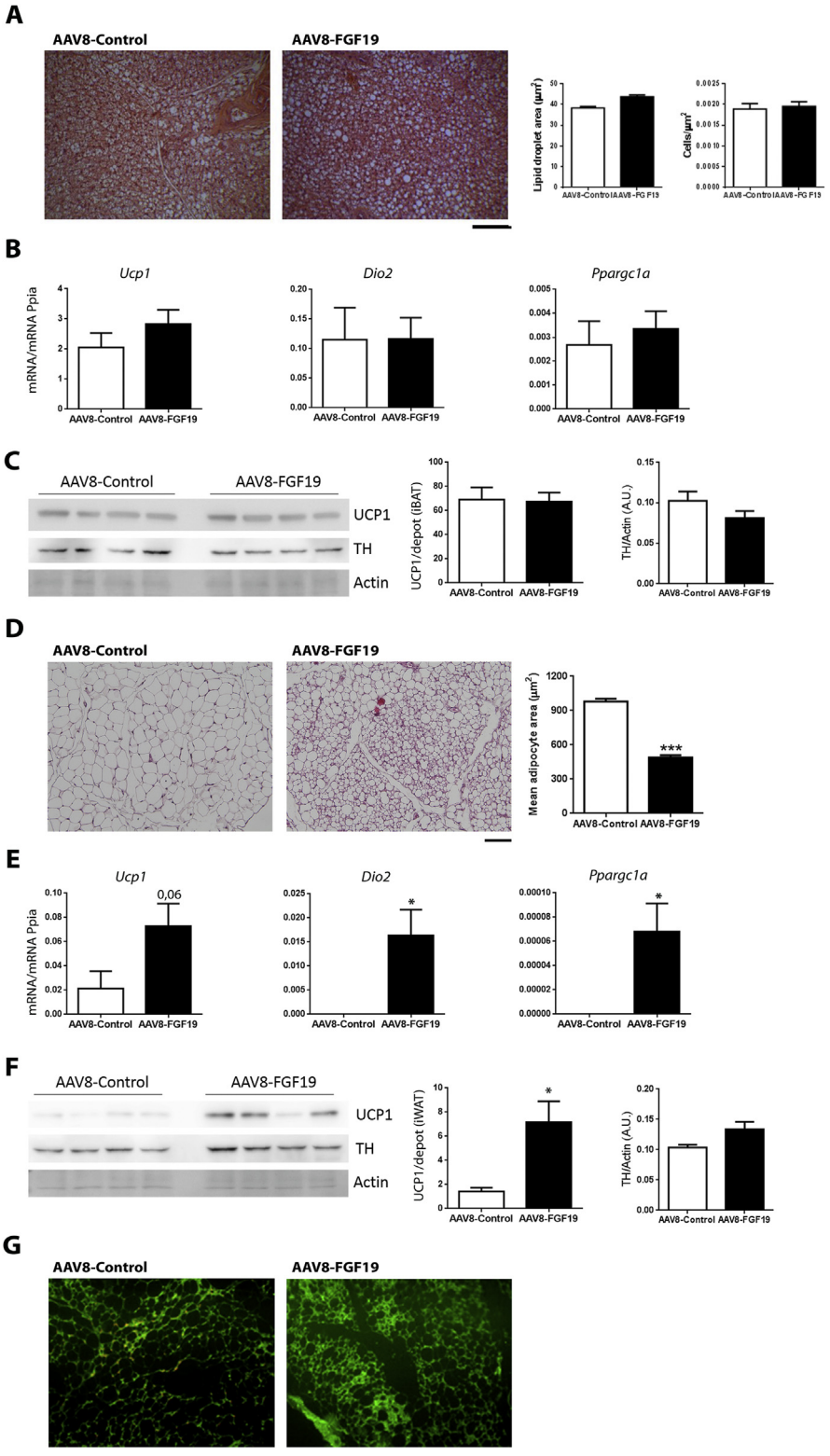

Figure 3: Overexpression of human FGF19 promotes browning of subcutaneous white adipose tissue in mice. All data correspond to 3-month-old C57BL/6J mice subjected to adeno-associated virus-mediated FGF19 overexpression for 3 weeks. Representative hematoxylin and eosin-stained histological sections of (A) BAT (20×) and quantification of lipid droplet areas and BAT density, (D) iWAT (10×), and quantification of adipocyte areas. Scale: 100 µm mRNA levels of *Ucp1*, *Dio2*, and *Ppargc*1a in (B) BAT and (E) iWAT. Representative pictures of UCP1 protein immunodetection and protein levels of UCP1 per depot in (C) BAT and (F) iWAT. Actin immunodetection was used as a loading control. (G) UCP1 (green) and nucleus (red) immunohistofluorescence staining in iWAT. Bars indicate mean ± SEM (n = 6). *P ≤ 0.05 denotes statistical significance for comparisons between AAV8-control and AAV8-FGF19 analyzed by Student's t-test.

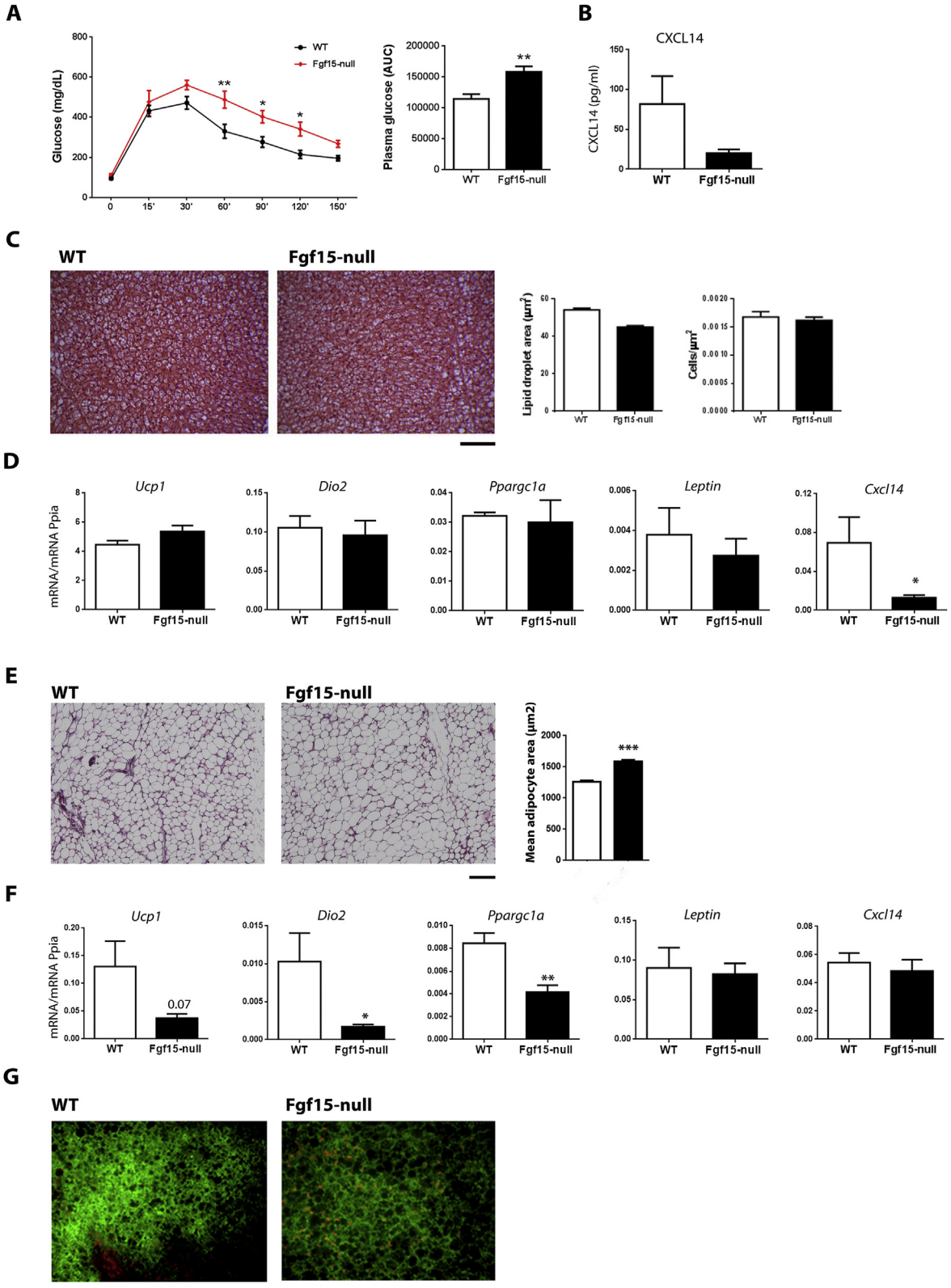

Figure 4: The lack of FGF15 reduces browning of subcutaneous WAT in mice. All data corresponded to 3-month-old WT or Fgf15-null mice housed at 22 °C. (A) Glucose tolerance test (GTT) profile (left) and area under the GTT curve (right). (B) CXCL14 levels in plasma. Representative hematoxylin and eosin-stained histological sections of (C) BAT (20×) and quantification of lipid droplet areas and BAT density, and (E) iWAT (10×) and quantification of adipocyte areas. Scale 100 µm mRNA levels of *Ucp1*, *Dio2*, *Ppargc1a*, *leptin*, and *Cxcl14* in (D) BAT and (F) iWAT. (G) UCP1 (green) and nucleus (red) immunohistofluorescence staining in iWAT. Bars indicate mean ± SEM (n = 6). *P ≤ 0.05, **P ≤ 0.01, and ***P ≤ 0.001 denote statistical significance for comparisons between WT and Fgf15-null mice analyzed by Student's t-test.

protein level of UCP1 (Figure 2C), and tyrosine hydroxylase (TH) protein abundance, indicative of the extent of sympathetic innervation. However, we observed a marked increase in subcutaneous WAT browning as reflected by an augmented number of multilocular adipocytes (Figure 2D), increased expression of thermogenesis- and beige-related marker genes such as *Ucp1*, *Dio2*, and *Ppargc1a* (Figure 2E), and strong induction of UCP1 protein levels (Figure 2F). The levels of TH protein also tended to increase in iWAT in response to increased FGF15 (Figure 2F). Increased FGF15 also led to a high UCP1-expressing adipocyte mass in iWAT, as assessed by immunohistofluorescence (Figure 2G).

To complement the previously described study, we used a similar approach to analyze the effects of adeno-associated virus serotype 8 (AAV8)-mediated overexpression of human FGF19 in mouse liver and its subsequent secretion over a 3-week period. In this case, the availability of reliable commercial FGF19 antibodies allowed us to determine that the injection of AAV8-FGF19 in the mice yielded a plasma concentration of FGF19 of 170 $\pm$ 18 pg/ml, which was in range of that observed in healthy humans (296 $\pm$ 36 pg/ml). This expression of FGF19 was associated with some reduction in the sizes of iBAT and WAT depots without any major change in body weight (Supplemental Table 4). Glycemia and triglyceridemia were also unaltered, whereas insulin levels trended lower in the AAV8-FGF19-injected mice. Similar to the results described above, hepatic *Cyp7a1* was massively repressed in the AAV8-FGF19-injected mice, demonstrating that the expected biological action of FGF15 was mimicked at this level by overexpression of human FGF19. Hepatic *Fgf21* expression and the circulating level of FGF21 were not altered by FGF19 overexpression (Supplemental Table 4).

AAV8-FGF19 injection did not significantly modify iBAT in terms of its histological appearance (Figure 3A), gene expression levels of *Ucp1*, *Dio2*, *Ppargc1a* (Figure 3B), and *Cxcl14* (Supplemental Table 4), or protein level of UCP1 and TH (Figure 3C). In contrast, subcutaneous WAT experienced a dramatic "browning" response to FGF19 overexpression, with a marked appearance of smaller and typical multilocular beige adipocytes (Figure 3D), marked induction of *Ucp1*, *Dio2*, and *Ppargc1a* expression (Figure 3E), a significant upregulation of the UCP1 protein level (Figure 3F) and the abundance of UCP1-expressing adipocytes (Figure 3G), and a trend to increased TH levels (Figure 3F) in iWAT. Together, these findings indicate that increase in the protein levels of FGF15 and FGF19 promotes the browning of subcutaneous WAT.

3.3. Impaired WAT browning in Fgf15-null mice

The results described above prompted us to investigate the role of the FGF15/19 system on brown and beige adipose tissue biology using the FGF15-null mouse model, which had not previously been used for this purpose. The initial report on the Fgf15-null mice indicated that they lacked viability [23]. However, subsequent work found that invalidation of FGF15 in a mixed C57BL/6/129/Sv background resulted in viable Fgf15-null mice, and these mice were used to study the role of FGF15 in hepatic function [18]. This model enabled us to investigate for the first time how FGF15 loss of function impacts adipose tissues.

The Fgf15-null mice housed at 21 °C showed mildly reduced adiposity; this was demonstrated by reduced sizes of iWAT and epididymal WAT (eWAT) (Supplemental Table 5) without significant alterations in the gross body weight. Relative to wild-type (WT) mice, the Fgf15-null mice had unaltered food energy intake, glycemia, or insulinemia, but showed markedly impaired glucose tolerance (Figure 4A). There was no significant difference in the levels of triglycerides or FGF21, although the latter showed a nonsignificant tendency to be upregulated in the Fgf15-null mice ($P = 0.06$) (Supplemental Table 5). Circulating levels of CXCL14 were also reduced in the FGF15-null mice (Figure 4B).

Hepatic gene expression analysis indicated that the Fgf15-null mice exhibited an intense induction of the *Cyp7a1* gene transcript (WT, 42.0 $\pm$ 8.2 vs. Fgf15-null, 170.0 $\pm$ 42.0, and $P < 0.01$). This was consistent with the reported ability of FGF15 to repress this key gene of bile acid synthesis [18] and verified the biological effectiveness of FGF15 loss of function in the Fgf15-null mouse model. However, the circulating total bile acid levels were not significantly altered (Supplemental Table 5).

Histological analysis of BAT from the Fgf15-null mice did not reveal any major changes (Figure 4C) regarding lipid droplet size or the number of cells, and the transcript levels for key genes related to BAT-mediated thermogenesis, such as *Ucp1*, *Dio2*, and *Ppargc1a*, were not significantly modified (Figure 4D). The transcript level of leptin (an indirect marker of adiposity) was also unchanged in the BAT of the Fgf15-null mice. Assessment of heat production at the interscapular BAT site by infrared thermography did not reveal any significant difference between the Fgf15-null and WT mice (Supplemental Fig. S1A). However, the expression of the batokine *Cxcl14* was dramatically downregulated in BAT from the FGF15-null mice (Figure 4D).

In contrast, histological examination of subcutaneous iWAT revealed that the Fgf15-null mice were characterized by a larger adipocyte size (Figure 4E) and an important reduction in the transcript levels of genes related to adaptive thermogenesis and beige phenotypes, such as *Ucp1*, *Dio2*, and *Ppargc1a* (Figure 4F). Moreover, immunohistofluorescence-based assessment of UCP1-expressing adipocyte mass revealed a reduction in iWAT from the Fgf15-null mice (Figure 4G). Thus, the Fgf15-null mice housed under a mild thermogenic challenge (21 °C) showed a reduced extent of browning in iWAT.

3.4. Impaired adaptive plasticity of WAT to thermogenic challenges in Fgf15-null mice

In light of the altered morphology and signs of impaired WAT browning in the FGF15-null mice under basal and 21°C-housed conditions, we analyzed the responsiveness of mice lacking FGF15 to adaptive thermogenic challenges. For this purpose, we exposed the mice to a 1-week adaptation at an environmental temperature of 4 °C, which confers a high requirement for thermogenesis. Both the WT and Fgf15-null mice could adapt to this cold challenge without any compromise in their viability or overt sign of hypothermia. Of note, cold exposure in the WT mice did not alter Fgf15 expression levels in the ileum (Supplemental Table 6). After the 1-week cold challenge, the Fgf15-null mice showed a non-significant trend toward maintaining larger masses of iWAT and eWAT relative to the WT mice (Supplemental Table 6). Whereas glycemia was not altered by the lack of FGF15 in the cold-exposed mice, insulinemia was much higher in the cold-exposed Fgf15-null mice than the cold-exposed WT mice (Supplemental Table 6). In fact, while insulin sensitization is known to occur in response to cold [24], the Fgf15-null mice were far less able than the WT mice to reduce insulin levels in response to 4 °C.

We analyzed the capacity of the mice maintained at 21 °C to adapt to thermoneutrality (30 °C) as a second reciprocal model of adaptive adipose tissue plasticity (in this case, suppression of thermogenic activity) [25,26]. The body weight was not altered in the Fgf15-null mice relative to the WT mice after both groups were exposed to 30 °C, although the masses of the various WAT depots were significantly higher in the Fgf15-null mice, showing statistical significance for eWAT (Supplemental Table 6). The iBAT mass was also higher,

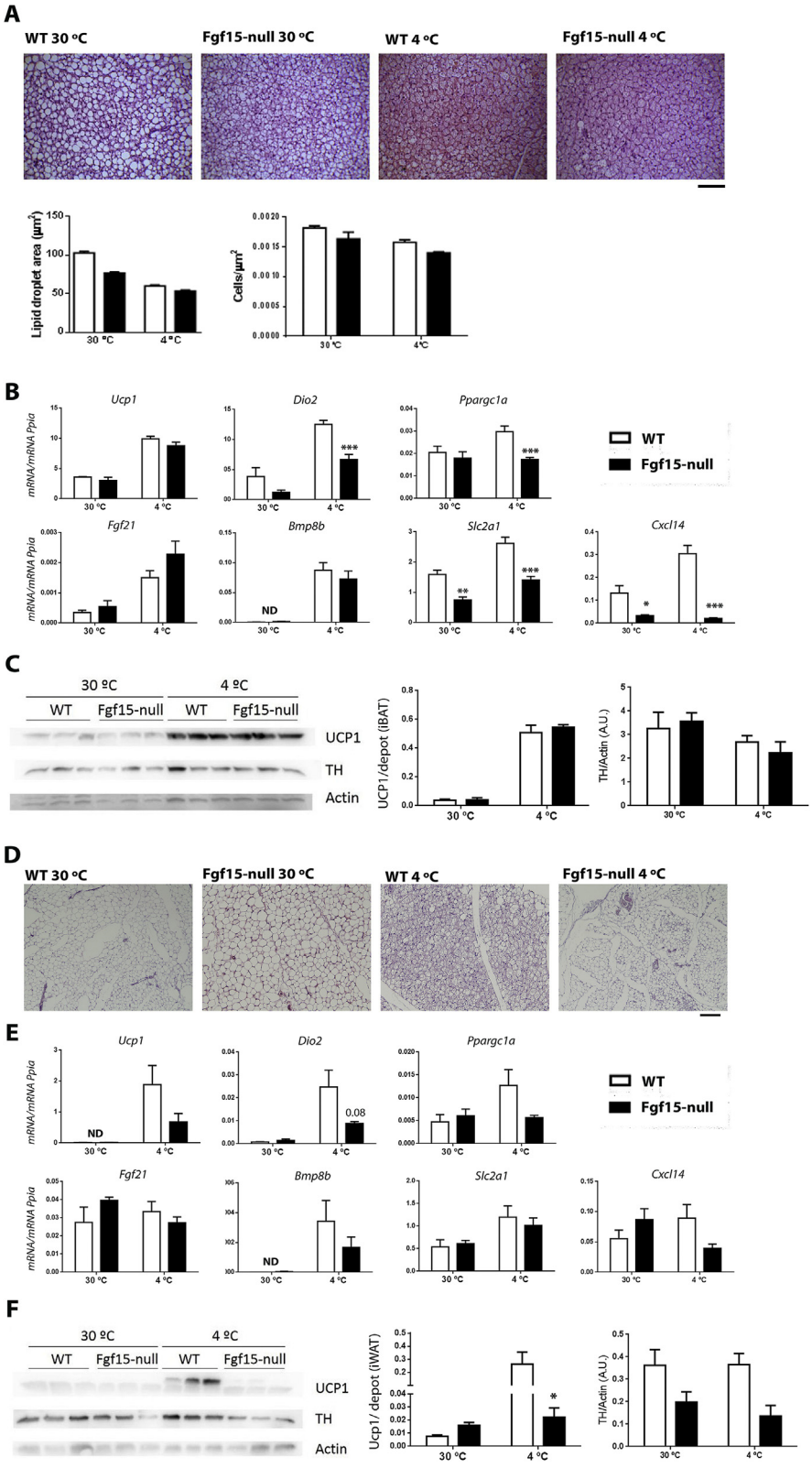

Figure 5: Fgf15-null mice exhibit impaired browning of subcutaneous WAT in response to cold. All data corresponded to 3-month-old WT or Fgf15-null mice housed at 4 °C or 30 °C for 1 week. Representative hematoxylin and eosin-stained histological sections of (A) BAT (20×) and (D) iWAT (10×). Scale 100 µm mRNA levels of *Ucp1*, *Dio2*, *Ppargc1a*, *Fgf21*, *Bmp8b*, *Slc2a1*, and *Cxcl14* in (B) BAT and (E) iWAT. Representative images of UCP1 protein immunodetection and protein levels of UCP1 per depot in (C) BAT and (F) iWAT. Ponceau staining was used as a loading control. Bars indicate mean ± SEM (n = 6). *P ≤ 0.05, **P ≤ 0.01, and ***P ≤ 0.001 denote statistical significance for comparisons between WT and Fgf15-null mice analyzed by two-way ANOVA test with Tukey's post hoc correction.

likely due to increased fat mass. Regarding systemic parameters, there was no significant difference in the levels of triglycerides, but a reduction in FGF21 levels in the Fgf15-null mice vs the WT mice was found when both groups were adapted to thermoneutrality (Supplemental Table 6).

Although there were no significant alterations in the histological morphology (Figure 5A), the capacity of BAT to respond to cold (4 °C) showed some signs of impairment in the Fgf15-null mice as demonstrated by reduced transcript levels of *Dio2*, *Ppargc1a*, and *Slc2a1* (Figure 5B). However, the levels of *Ucp1* transcript (Figure 5B), UCP1 protein, and TH protein (Figure 5C) in the cold-exposed Fgf15-null mice relative to the cold-exposed WT mice did not significantly change. The heat production at the interscapular BAT site, which was assessed by infrared thermography, was not significantly different in the 4°C-exposed Fgf15-null mice vs the 4°C-exposed WT mice (Supplemental Fig. S1B). However, the expression of *Cxcl14* was markedly impaired in BAT from the Fgf15-null mice maintained at 4 °C (Figure 5B).

In the mice exposed to thermoneutral conditions (30 °C), the histological analysis and thermogenesis-related gene expression profiles supported the idea that only minor changes occurred in the absence of FGF15 in BAT. Among the tested markers, significant decreases were seen solely in *Slc2a1* and *Cxcl14* (Figure 5B).

In contrast, iWAT experienced much more dramatic changes due to thermogenic challenges in the Fgf15-null vs WT mice. Histological analysis revealed a massive "browning" (appearance of multilocular beige-type adipocytes) in iWAT from the WT mice exposed to 4 °C, whereas much less browning appeared in the Fgf15-null mice exposed to cold (Figure 5D).

The inductions of *Ucp1*, *Dio2*, and *Ppargc1a* were significantly impaired in iWAT from the cold-exposed Fgf15-null mice (Figure 5E). Relative UCP1 protein levels and absolute UCP1 protein levels per iWAT depot were significantly reduced in iWAT from the Fgf15-null mice (Figure 5F), confirming that adaptive browning of iWAT was impaired in the Fgf15-null mice. TH levels were also reduced in the Fgf15-null mice relative to the WT mice in response to cold, indicating that the enhanced sympathetic innervation associated with WAT browning was impaired due to the lack of FGF15. The expression levels of genes involved in adaptive thermogenesis (for example, *Ucp1*, *Dio2*, and *Bmp8b*) were almost undetectable in iWAT from the 30°C-exposed WT and Fgf15-null mice (Figure 5E), while *Slc2a1* and *Cxcl14* were detectable but did not show any difference due to the absence of FGF15 at in the mice maintained at 30 °C.

Similar observations were obtained for eWAT, a visceral WAT depot that is less prone to browning than subcutaneous WAT. Although 1-week exposure to a 4 °C ambient temperature did not yield any overt signs of morphological browning of eWAT in the WT or Fgf15-null mice (Supplemental Fig. S2A), gene expression analysis revealed that the mRNAs for *Ucp1* and *Dio2* were significantly induced in the WT mice but not the Fgf15-null mice (Supplemental Fig. S2B). On the basis of our results, we conclude that experimentally induced suppression of FGF15 in mice impairs the capacity to induce WAT browning.

We determined whether the expression of cellular components of the FGF15 responsiveness machinery in adipose tissues was affected by thermal stress and/or FGF15 gene invalidation. Cold exposure (4 °C) resulted in a much higher expression of KLB (but not FGFR1 or FGFR4) in iWAT from the WT and Fgf15-null mice. No such effect of cold was found in BAT.

As complementary data, we determined the expression of a panel of marker genes of an M1 pro-inflammatory phenotype (*Nos2*, *Tnfa*, *Il6*, and *Ccl2*) and an alternative M2-type phenotype (*Arg1*, *Mrc1*, *Il10*, and *Arg1*/*Nos2* ratio) of infiltrating macrophages in mouse adipose depots in the distinct gain- and loss-of-function experimental models (Supplemental Tables 8—11). Despite minor significant changes, no systematic patterns of alteration were found in response to FGF15/19-related experimental manipulations, thus indicating that modulation of pro- or anti-inflammatory status with adipose depots was not a key component of the FGF15-mediated effects.

4. DISCUSSION

In this study, we found that the level of FGF19 was positively associated with the expression of UCP1 (a key marker gene of thermogenic activity and browning of adipose tissue) in a human cohort spanning a wide range of body weights. This prompted us to use mouse models to study the role of FGF15/19 as a potential mediator of intestine-originating signaling to control the browning of adipose tissues.

There are important limitations when studying FGF15/19's role in energy metabolism using rodent models. For example, there is a lack of tools for antibody-based quantification of FGF15 in rodents; only complex methods involving capture by anti-peptide antibodies combined with selected reactions monitoring mass spectrometry have achieved such quantification [27]. Other limitations include the lack of recombinant FGF15 and the high mortality observed in the first mouse models of FGF15 gene invalidation [23]. These issues have dampened experimental studies attempting to establish FGF15's actual physiological role in adipose tissue plasticity. Herein, we describe the first study using a FGF15-null mouse model and FGF15 gain-of-function approaches to show that FGF15 plays a key role in adaptive WAT browning.

Previous studies have shown that overexpression or treatment of mice with high levels of human FGF19 can improve metabolism, increase energy expenditure, cause mild effects on BAT activity [28,29], and promote WAT browning [30]. However, the heterologous nature of these studies and the large divergence between human FGF19 and mouse FGF15 made it difficult to appreciate the actual physiological role of the FGF19/15 system in adipose tissue plasticity. In this study, we established the presence of these effects in a totally specified homologous system based on overexpressing FGF15 in mice. However, this pharmacological approach based on high levels of overexpression requires further studies to determine the actual physiological role of the FGF19/15 system in relation to adipose tissue plasticity.

Our findings indicated that the absence of FGF15 severely impaired the capacity of WAT to undertake browning in response to thermogenic challenges, whereas it impacted BAT activity in a more moderate manner. This pattern of alterations mirrored the findings in mice subjected to an experimentally induced increase in FGF15. The preferential targeting of WAT also involved the modulation of sympathetic innervation as demonstrated by TH data. The reasons for the preferential sensitivity of WAT-versus-BAT to FGF15/19-mediated effects were unclear, but data on increased expression of KLB in WAT (but not BAT) in response to cold may contribute to sensitization to FGF15/19-mediated signaling. Of note, a previous report using a heterologous model of FGF19 treatment of mice [30] showed increased energy expenditure associated with an intense induction of UCP1 expression in WAT, indicative of browning, which was concordant with our findings. Interestingly, the induction of UCP1 was found to be required for the thermogenic action of FGF19 treatment but not for FGF19-mediated obesity protection. These findings highlight the importance of the FGF19/15 pathway in the regulation of energy metabolism and the complex mechanisms involved, ranging from the control of adipose

tissue plasticity to impaired intestinal energy absorption elicited by altered bile acid homeostasis [30].

Our current study did not allow us to fully establish the mechanisms by which FGF15 controls WAT browning. Direct effects of FGF15 on brown/beige adipocytes or pre-adipocytes cannot be ruled out, although the existing evidence suggests that indirect effects are more important. Some reports have suggested that FGFR1 receptors present on adipose cells can mediate the cellular action of FGF15/19 [31]. However, FGFR4, which is the main receptor accounting for the effects of FGF15/19 [32], is poorly expressed in brown/beige adipocytes and pre-adipocytes [1]. We found that browning-susceptible human pre-adipocyte cells were unable to acquire a browning phenotype in response to FGF19 in vitro (unpublished data). Thus, distinct indirect mechanisms are likely to account for the effects of FGF5/19 on WAT browning.

Bile acids are known to activate BAT, but suppression of FGF15 either failed to alter (this study) or increase [18] the level of bile acids, which is consistent with FGF15's role as a negative regulator of bile acid biosynthesis [2]. Thus, bile acid-mediated alterations are not likely to account for the positive relationship between FGF15 and WAT browning. However, studies based on the direct administration of FGF19 to distinct brain regions that express FGFR1 and KLB revealed positive effects on metabolism, including improved glucose tolerance, increased energy expenditure, and BAT activation [33]. Thus, it cannot be ruled out that the action of FGF15 in promoting WAT browning may involve indirect centrally mediated mechanisms through the control of sympathetic activity upon adipose tissue, which would be consistent with our data on altered TH expression in WAT depots. However, one of the most affected genes in BAT from FGF15-null mice is CXCL14, a batokine that contributes to WAT browning when it is secreted by BAT following a thermogenic stimulus [34]. CXCL14 blood levels were concomitantly reduced in several of our experimental models in FGF15-null mice. However, gain-of-function experiments did not trigger increased CXCL14 expression parallel to the induction of WAT browning, which may indicate that basal physiological CXCL14 expression is permissive for FGF15/19's effects. However, we did not find evidence that modulation of pro- or anti-inflammatory status within adipose depots as expected for CXCL14 action [34] was a key component of the FGF15-mediated effects. In any case, future research is warranted to determine the precise involvement of CXCL14 in the FGF15-mediated browning of WAT.

Multiple reports in humans have revealed a negative correlation between FGF19 levels and obesity and type II diabetes [20,35]. Considering that WAT browning protects against metabolic diseases in rodent models [36,37] and possibly in humans [38,39,40,41], our findings suggest that FGF15/19 may contribute to a mechanism for intestine-to-adipose tissue communication, thereby promoting energy expenditure and metabolic health. In fact, the systemic effects of our loss- and gain-of-function manipulations of FGF15 in mice (i.e., reduced glucose tolerance and impaired cold-induced insulin sensitization observed in the FGF15-null mice) support this notion. Further research is needed to ascertain how the positive actions of FGF15 on the browning of WAT could contribute to disease prevention and metabolic health improvement in clinical settings and experimental models.

5. CONCLUSIONS

Our study reports that the circulating level of FGF19 correlates with the levels of the brown/beige gene marker UCP1 in subcutaneous adipose tissue of humans. In addition, a deficit in FGF15 impairs browning of subcutaneous WAT after cold challenges (4 °C and 21 °C), while overexpression of FGF15 and FGF19 promotes browning in mice. FGF15/19 constitutes an intestine-originating signaling component that is involved in controlling adipose tissue plasticity during thermogenic adaptations.

FUNDING

Funding from the Ministry of Science and Innovation (SAF2017-85722R); Health Research Fund, Carlos III Health Institute (PI17-00420), co-financed by the European Regional Development Fund (ERDF); the Marató de TV3 Foundation (201612-30/31); the Fundación Bancaria La Caixa (Hepacare Project); the M. Torres Foundation; and the Eugenio Rodriguez Pascual Foundation (to IU, CB, and MAA) is acknowledged.

AUTHOR CONTRIBUTIONS

S.M-R., F.V., and A.G-N. conducted and analyzed the experiments in FGF15-null mice. I.U., S.M-R., C.B., MA.A., and A.G-N. performed and analyzed the experiments in adenovirus- and AAV vector-injected mice. M.S-M., JM.M-N., and JM.F-R obtained and analyzed data from human subjects. A.G-N., MA.A., M.G., and F.V conceived the study and interpreted the data. A.G-N. and F.V. wrote the manuscript. All authors critically reviewed and edited the manuscript.

ACKNOWLEDGMENTS

The authors acknowledge R. Barbero (CIMA) for his support in the mouse in vivo studies and A. Peró and M. Morales for technical support. We also want to particularly acknowledge the patients, the FATBANK platform promoted by the CIBEROBN, and the IDIBGI Biobank (Biobanc IDIBGI, B.0000872) integrated in the Spanish National Biobanks Network for their collaboration and coordination. We are indebted to the Biobank core facility of the Institute of Biomedical Research August Pi i Sunyer (IDIBAPS) for the technical help.

CONFLICT OF INTEREST

None declared.

APPENDIX A. SUPPLEMENTARY DATA

Supplementary data to this article can be found online at https://doi.org/10.1016/j.molmet.2020.101113.

REFERENCES

[1] Kurosu, H., Choi, M., Ogawa, Y., Dickson, A.S., Goetz, R., Eliseenkova, A.V., et al., 2007. Tissue-specific expression of betaKlotho and fibroblast growth factor (FGF) receptor isoforms determines metabolic activity of FGF19 and FGF21. Journal of Biological Chemistry 282(37):26687–26695.

[2] Inagaki, T., Choi, M., Moschetta, A., Peng, L., Cummins, C.L., McDonald, J.G., et al., 2005. Fibroblast growth factor 15 functions as an enterohepatic signal to regulate bile acid homeostasis. Cell Metabolism 2(4):217–225.

[3] Kir, S., Beddow, S.A., Samuel, V.T., Miller, P., Previs, S.F., Suino-Powell, K., et al., 2011. FGF19 as a postprandial, insulin-independent activator of hepatic protein and glycogen synthesis. Science 331(6024):1621–1624.

[4] Alvarez-Sola, G., Uriarte, I., Latasa, M.U., Fernandez-Barrena, M.G., Urtasun, R., Elizalde, M., et al., 2017. Fibroblast growth factor 15/19 (FGF15/19) protects from diet-induced hepatic steatosis: development of an FGF19-

based chimeric molecule to promote fatty liver regeneration. Gut 66(10): 1818–1828.
[5] Alvarez-Sola, G., Uriarte, I., Latasa, M.U., Urtasun, R., Barcena-Varela, M., Elizalde, M., et al., 2017. Fibroblast growth factor 15/19 in hepatocarcinogenesis. Digestive Diseases 35(3):158–165.
[6] Giralt, M., Villarroya, F., 2013. White, brown, beige/brite: different adipose cells for different functions? Endocrinology 154(9):2992–3000.
[7] Cereijo, R., Villarroya, J., Villarroya, F., 2015. Non-sympathetic control of brown adipose tissue. International Journal of Obesity Supplements 5(Suppl 1): S40–S44.
[8] Keipert, S., Kutschke, M., Ost, M., Schwarzmayr, T., van Schothorst, E.M., Lamp, D., et al., 2017. Long-term cold adaptation does not require FGF21 or UCP1. Cell Metabolism 26(2):437–446.
[9] Mestdagh, R., Dumas, M.E., Rezzi, S., Kochhar, S., Holmes, E., Claus, S.P., et al., 2012. Gut microbiota modulate the metabolism of brown adipose tissue in mice. Journal of Proteome Research 11(2):620–630.
[10] Moreno-Navarrete, J.M., Fernandez-Real, J.M., 2019. The gut microbiota modulates both browning of white adipose tissue and the activity of brown adipose tissue. Reviews in Endocrine & Metabolic Disorders 20(4):387–397.
[11] Li, B., Li, L., Li, M., Lam, S.M., Wang, G., Wu, Y., et al., 2019. Microbiota depletion impairs thermogenesis of Brown adipose tissue and browning of white adipose tissue. Cell Reports 26(10):2720–2737.
[12] Xiao, H., Kang, S., 2020. The role of the gut microbiome in energy balance with a focus on the gut-adipose tissue Axis. Frontiers in Genetics 11:297.
[13] Beiroa, D., Imbernon, M., Gallego, R., Senra, A., Herranz, D., Villarroya, F., et al., 2014. GLP-1 agonism stimulates brown adipose tissue thermogenesis and browning through hypothalamic AMPK. Diabetes 63(10):3346–3358.
[14] Li, Y., Schnabl, K., Gabler, S.M., Willershauser, M., Reber, J., Karlas, A., et al., 2018. Secretin-activated Brown fat mediates prandial thermogenesis to induce satiation. Cell 175(6):1561–1574.
[15] Batterham, R.L., Cummings, D.E., 2016. Mechanisms of diabetes improvement following bariatric/metabolic surgery. Diabetes Care 39(6):893–901.
[16] Vijgen, G.H., Bouvy, N.D., Teule, G.J., Brans, B., Hoeks, J., Schrauwen, P., et al., 2012. Increase in brown adipose tissue activity after weight loss in morbidly obese subjects. Journal of Clinical Endocrinology & Metabolism 97(7): E1229–E1233.
[17] Bozadjieva, N., Heppner, K.M., Seeley, R.J., 2018. Targeting FXR and FGF19 to treat metabolic diseases-lessons learned from bariatric surgery. Diabetes 67(9):1720–1728.
[18] Uriarte, I., Fernandez-Barrena, M.G., Monte, M.J., Latasa, M.U., Chang, H.C., Carotti, S., et al., 2013. Identification of fibroblast growth factor 15 as a novel mediator of liver regeneration and its application in the prevention of post-resection liver failure in mice. Gut 62(6):899–910.
[19] Galarraga, M., Campion, J., Munoz-Barrutia, A., Boque, N., Moreno, H., Martinez, J.A., et al., 2012. Adiposoft: automated software for the analysis of white adipose tissue cellularity in histological sections. The Journal of Lipid Research 53(12):2791–2796.
[20] Gallego-Escuredo, J.M., Gomez-Ambrosi, J., Catalan, V., Domingo, P., Giralt, M., Fruhbeck, G., et al., 2015. Opposite alterations in FGF21 and FGF19 levels and disturbed expression of the receptor machinery for endocrine FGFs in obese patients. International Journal of Obesity 39(1):121–129.
[21] Zhou, M., Luo, J., Chen, M., Yang, H., Learned, R.M., DePaoli, A.M., et al., 2017. Mouse species-specific control of hepatocarcinogenesis and metabolism by FGF19/FGF15. Journal of Hepatology 66(6):1182–1192.
[22] Wei, K., Kuhnert, F., Kuo, C.J., 2008. Recombinant adenovirus as a methodology for exploration of physiologic functions of growth factor pathways. Journal of Molecular Medicine (Berlin) 86(2):161–169.
[23] Wright, T.J., Ladher, R., McWhirter, J., Murre, C., Schoenwolf, G.C., Mansour, S.L., 2004. Mouse FGF15 is the ortholog of human and chick FGF19, but is not uniquely required for otic induction. Developmental Biology 269(1): 264–275.
[24] Cannon, B., Nedergaard, J., 2004. Brown adipose tissue: function and physiological significance. Physiological Reviews 84(1):277–359.
[25] Kajimura, S., Saito, M., 2014. A new era in brown adipose tissue biology: molecular control of brown fat development and energy homeostasis. Annual Review of Physiology 76:225–249.
[26] Cairo, M., Campderros, L., Gavalda-Navarro, A., Cereijo, R., Delgado-Angles, A., Quesada-Lopez, T., et al., 2019. Parkin controls brown adipose tissue plasticity in response to adaptive thermogenesis. EMBO Reports 20(5).
[27] Katafuchi, T., Esterhazy, D., Lemoff, A., Ding, X., Sondhi, V., Kliewer, S.A., et al., 2015. Detection of FGF15 in plasma by stable isotope standards and capture by anti-peptide antibodies and targeted mass spectrometry. Cell Metabolism 21(6):898–904.
[28] Tomlinson, E., Fu, L., John, L., Hultgren, B., Huang, X., Renz, M., et al., 2002. Transgenic mice expressing human fibroblast growth factor-19 display increased metabolic rate and decreased adiposity. Endocrinology 143(5): 1741–1747.
[29] Fu, L., John, L.M., Adams, S.H., Yu, X.X., Tomlinson, E., Renz, M., et al., 2004. Fibroblast growth factor 19 increases metabolic rate and reverses dietary and leptin-deficient diabetes. Endocrinology 145(6):2594–2603.
[30] Antonellis, P.J., Droz, B.A., Cosgrove, R., O'Farrell, L.S., Coskun, T., Perfield, J.W., et al., 2019. The anti-obesity effect of FGF19 does not require UCP1-dependent thermogenesis. Molecular Metabolism 30:131–139.
[31] Yang, C., Jin, C., Li, X., Wang, F., McKeehan, W.L., Luo, Y., 2012. Differential specificity of endocrine FGF19 and FGF21 to FGFR1 and FGFR4 in complex with KLB. PloS One 7(3):e33870.
[32] Inagaki, T., Lin, V.Y., Goetz, R., Mohammadi, M., Mangelsdorf, D.J., Kliewer, S.A., 2008. Inhibition of growth hormone signaling by the fasting-induced hormone FGF21. Cell Metabolism 8(1):77–83.
[33] Lan, T., Morgan, D.A., Rahmouni, K., Sonoda, J., Fu, X., Burgess, S.C., et al., 2017. FGF19, FGF21, and an FGFR1/beta-Klotho-activating antibody act on the nervous system to regulate body weight and glycemia. Cell Metabolism 26(5): 709–718.
[34] Cereijo, R., Gavalda-Navarro, A., Cairo, M., Quesada-Lopez, T., Villarroya, J., Moron-Ros, S., et al., 2018. CXCL14, a Brown adipokine that mediates Brown-Fat-to-Macrophage communication in thermogenic adaptation. Cell Metabolism 28(5):750–763.
[35] Gomez-Ambrosi, J., Gallego-Escuredo, J.M., Catalan, V., Rodriguez, A., Domingo, P., Moncada, R., et al., 2017. FGF19 and FGF21 serum concentrations in human obesity and type 2 diabetes behave differently after diet- or surgically-induced weight loss. Clinical Nutrition 36(3):861–868.
[36] Stanford, K.I., Middelbeek, R.J., Townsend, K.L., An, D., Nygaard, E.B., Hitchcox, K.M., et al., 2013. Brown adipose tissue regulates glucose homeostasis and insulin sensitivity. Journal of Clinical Investigation 123(1):215–223.
[37] Wang, T.Y., Liu, C., Wang, A., Sun, Q., 2015. Intermittent cold exposure improves glucose homeostasis associated with brown and white adipose tissues in mice. Life Sciences 139:153–159.
[38] Saito, M., Okamatsu-Ogura, Y., Matsushita, M., Watanabe, K., Yoneshiro, T., Nio-Kobayashi, J., et al., 2009. High incidence of metabolically active brown adipose tissue in healthy adult humans: effects of cold exposure and adiposity. Diabetes 58(7):1526–1531.
[39] Chondronikola, M., Volpi, E., Borsheim, E., Porter, C., Annamalai, P., Enerback, S., et al., 2014. Brown adipose tissue improves whole-body glucose homeostasis and insulin sensitivity in humans. Diabetes 63(12):4089–4099.
[40] Sidossis, L., Kajimura, S., 2015. Brown and beige fat in humans: thermogenic adipocytes that control energy and glucose homeostasis. Journal of Clinical Investigation 125(2):478–486.
[41] Thyagarajan, B., Foster, M.T., 2017. Beiging of white adipose tissue as a therapeutic strategy for weight loss in humans. Hormone Molecular Biology and Clinical Investigation 31(2).

